nature medicine

SUPPLEMENTARY INFORMATION

https://doi.org/10.1038/s41591-018-0010-1

In the format provided by the authors and unedited.

Determinants of response and resistance to CD19 chimeric antigen receptor (CAR) T cell therapy of chronic lymphocytic leukemia

Joseph A. Fraietta[1,2,3], Simon F. Lacey[1,2,3,9], Elena J. Orlando[4,9], Iulian Pruteanu-Malinici[4], Mercy Gohil[2], Stefan Lundh[2], Alina C. Boesteanu[2], Yan Wang[2], Roddy S. O'Connor[2], Wei-Ting Hwang[5], Edward Pequignot[2], David E. Ambrose[2], Changfeng Zhang[2], Nicholas Wilcox[2], Felipe Bedoya[2], Corin Dorfmeier[2], Fang Chen[2], Lifeng Tian[2], Harit Parakandi[2], Minnal Gupta[2], Regina M. Young[2], F. Brad Johnson[1], Irina Kulikovskaya[2], Li Liu[2], Jun Xu[2], Sadik H. Kassim[4], Megan M. Davis[1,2], Bruce L. Levine[1,2], Noelle V. Frey[2,6], Donald L. Siegel[1,2,7], Alexander C. Huang[3,8], E. John Wherry[3,8], Hans Bitter[4], Jennifer L. Brogdon[4], David L. Porter[1,6], Carl H. June[1,2,3] and J. Joseph Melenhorst[1,2,3]*

[1]Department of Pathology and Laboratory Medicine, University of Pennsylvania, Philadelphia, PA, USA. [2]Center for Cellular Immunotherapies, University of Pennsylvania, Philadelphia, PA, USA. [3]Parker Institute for Cancer Immunotherapy at University of Pennsylvania, Philadelphia, PA, USA. [4]Novartis Institutes for BioMedical Research, Cambridge, MA, USA. [5]Department of Biostatistics and Epidemiology, University of Pennsylvania, Philadelphia, PA, USA. [6]Division of Hematology-Oncology, Department of Internal Medicine, University of Pennsylvania, Philadelphia, PA, USA. [7]Division of Transfusion Medicine and Therapeutic Pathology, University of Pennsylvania, Philadelphia, PA, USA. [8]Department of Microbiology, Perelman School of Medicine, University of Pennsylvania, Philadelphia, PA, USA. [9]These authors contributed equally: Simon F. Lacey and Elena J. Orlando. *e-mail: mej@upenn.edu**

SUPPLEMENTAL APPENDIX

Table of Contents

Supplemental Table 1: ***Demographics and baseline characteristics for CLL patients treated with CTL019.***

Characteristic	CR	PR_{TD}	PR	NR	*P* value
n	8	3	5	25	-
Sex*					
Number of Male Patients	7	3	5	18	0.54
Number of Female Patients	1	0	0	7	
Age at Infusion - Years (Median)**	62	61	66	62	0.69
Interquartile range (25%-75%)	(59 - 64)	(59 - 65)	(65 - 66)	(59 - 69)	
Number of Previous Therapies (Median)**	5	4	3	3	0.69
Interquartile range (25%-75%)	(3 - 5)	(2 - 7)	(2 - 4)	(3 - 5)	
% Baseline Peripheral B CLL Cells (Median)**	57	65	62	82	0.45
Interquartile range (25%-75%)	(57 - 93)	(14 - 65)	(31 - 70)	(62- 92)	
Baseline Absolute CD19+ B Cell Count (Cells/ml; Median)**	7,746	632	1,764	6,942	0.37
Interquartile range (25%-75%)	(1,781 - 21,446)	(612 - 652)	(7 - 3,868)	(1,164 -18,291)	
p53*					
Wildtype	2	1	2	11	0.34
Mutated	0	0	1	2	
Deleted	3	1	0	6	
Other	0	0	2	1	
Unknown	3	1	0	5	

P values were calculated using the * Fisher's exact test or the ** Kruskal-Wallis exact test.

Supplemental Table 7: ***Summary of pre- and post-expansion T-cell characteristics and CTL019 treatment dose.***

Characteristic	CR	PR_{TD}	PR	NR	*P* value
n	*8*	3	5	25	-
% CD3+CD45+ at Leukapheresis (Median)	10	34	22	13	0.27
Interquartile range (25%-75%)	(3.5 - 25)	(23 - 54)	(8 - 25)	(5.3 - 33)	
% CD3+CD4+CD45+ at Leukapheresis (Median)	5	40	12	7	0.09
Interquartile range (25%-75%)	(1.7 - 13)	(16 - 54)	(4.4 - 16)	(3.4 - 14)	
% CD3+CD8+CD45+ at Leukapheresis (Median)	2	11	7	4	0.10
Interquartile range (25%-75%)	(1.4 - 4)	(10.6 - 16)	(4.3 - 11)	(0.9 - 9)	
% CD3+CD45+ Post-expansion (Median)	99.0	98.5	98.8	98.1	0.55
Interquartile range (25%-75%)	(98.6 - 99.5)	(96.5 - 99.5)	(97.8 - 99.2)	(97.3 - 99.0)	
% CD3+CD4+CD45+ Post-expansion (Median)	74	81	84	82	0.28
Interquartile range (25%-75%)	(63 - 79)	(72 - 83)	(82.7 - 88.2)	(73 - 90)	
% CD3+CD8+CD45+ Post-expansion (Median)	22	21	21	16	0.57
Interquartile range (25%-75%)	(17 - 38)	(16 - 28)	(16 - 26)	(9 - 25)	
% CAR (Median)	24	17.7	23.7	19	0.29
Interquartile range (25%-75%)	(18 - 26)	(17.3 - 28)	(22.6 - 39)	(10 - 26)	
Total Number of Infused CTL019 Cells (Median)	2×10^8	9×10^7	2×10^8	4×10^7	0.36
Interquartile range (25%-75%)	(8×10^7 - 6×10^8)	(2×10^7 - 3×10^8)	(1×10^8 - 4×10^8)	(2×10^7 - 3×10^8)	
Total CTL019 Dose (Cell Number/kg; Median)	3×10^6	9×10^5	2×10^6	6×10^5	0.33
Interquartile range (25%-75%)	(8×10^5 - 7×10^6)	(2×10^5 - 3×10^6)	(1×10^6 - 5×10^6)	(3×10^5 - 3×10^6)	

P values were calculated using the Kruskal-Wallis exact test.

Supplemental Table 9: ***Peak serum cytokine levels in the first twenty-eight days post-CAR T-cell infusion.***

Circulating Cytokine (pg/ml)	CR	PR_{TD}	PR	NR
n	8	3	5	25
IL-15 - median	180	206	47	61
Interquartile range (25%-75%)	(126 - 429)	(182 - 417)	(7 - 210)	(3 - 169)
IL-7 - median	17	43	22	8
Interquartile range (25%-75%)	(4 - 31)	(9 - 142)	(2* - 40)	(1* - 16)
IL-2 - median	3.4	13	3.6	1.4
Interquartile range (25%-75%)	(2.3* - 7)	(0.9* - 15)	(1.3* - 4.0)	(0.8* - 3.2)
IL-6 - median	243	2,608	41	23
Interquartile range (25%-75%)	(28 - 376)	(134 - 4,519)	(22 - 278)	(10 - 60)

*Extrapolated value; below limit of detection

Supplemental Table 10: ***Antibodies used for flow cytometry.***

Specificity	Clone	Conjugate	Supplier
CD3	OKT3, SK7	Brilliant Violet (BV) 605, Allophycocyanin (APC) H7	BioLegend
CAR19	136.20.1	Alexa Fluor (AF) 647	Kind gift of B. Jena and L. Cooper (MD Anderson Cancer Center)
CD19	HIB19	Phycoerythrin (PE) Cy7	BioLegend
CD20	2H7	APCH7	Becton Dickinson (BD)
STAT3 (pY705)	4/P-STAT3	PE	Becton Dickinson (BD)
CD8	RPA-T8	BV650	BioLegend
CD4	OKT4	BV785	BioLegend
CCR7	150503	FITC, PECF594	Becton Dickinson (BD)
CD27	1A4CD27, O323	PECy7, BV711	Beckman Coulter, BioLegend
CD45RO	UCHL1	PE, BV570, BV605	BioLegend
CD28	L293	BV605	Becton Dickinson (BD)
CD127	A019D5	BV711	BioLegend
HLA-DR	G46-6	FITC	Becton Dickinson (BD)
KLRG1	2F1/KLRG1	PE	BioLegend
CD95	DX2	PECy5	BioLegend
PD-1	EH12.2H7	BV421	BioLegend
TIM-3	F38-2E2	PE	BioLegend
LAG-3	3DS223H	PECy7	eBioscience
CD57	HCD57	FITC	BioLegend
Granzyme B	GB11	PECy5.5	Invitrogen
Ki-67	B56	AF700	Becton Dickinson (BD)
gp130	28126	PE	R&D Systems

Supplemental Figure 1: ***Principal component analysis (PCA) demonstrates genome-wide changes in CAR T-cells from patients belonging to each response category.*** Projection of transcriptomic data corresponding to CTL019 infusion products from patients in each response category (CR, n = 5; PR_{TD}, n = 3; PR, n = 5; NR, n = 21) onto the first two principal components. 95% confidence ellipses are drawn around samples classified into two clusters as determined by k-means clustering. The percentage of variation explained by each component is provided in the axis labels.

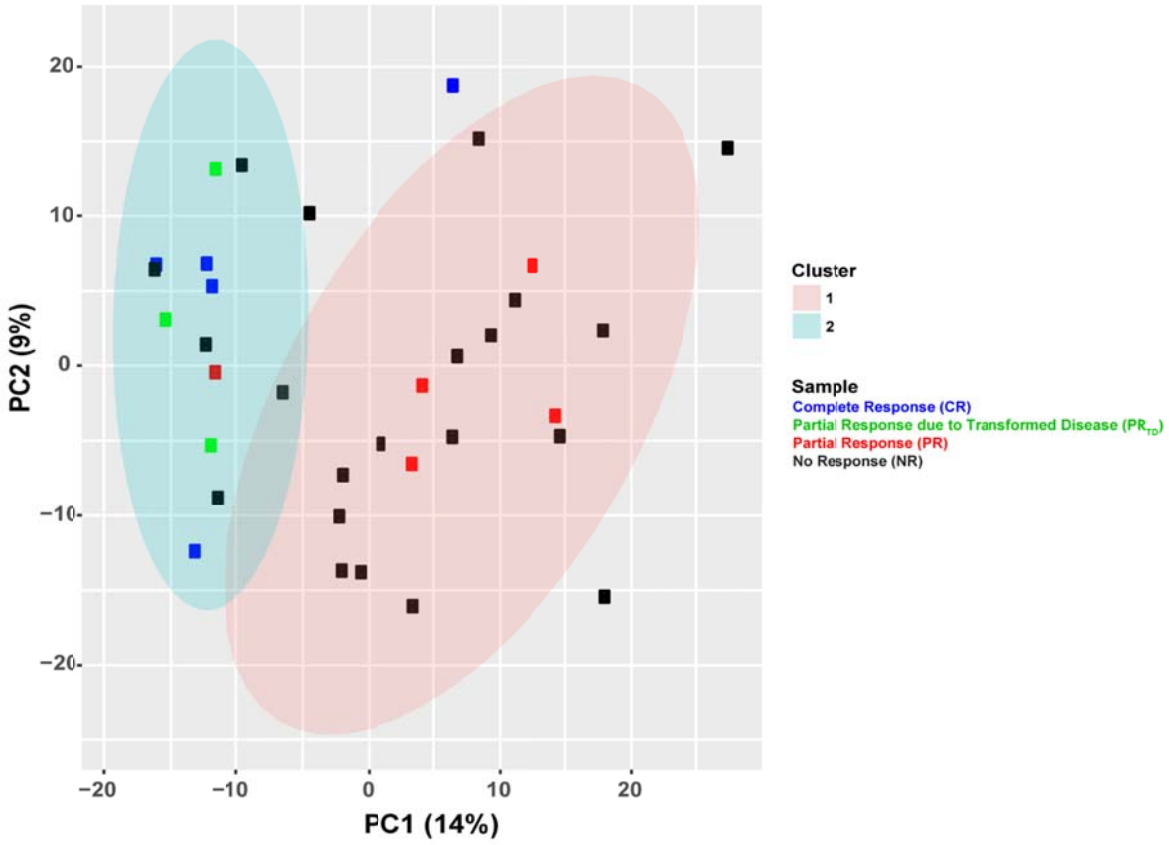

Supplemental Figure 2: ***Metabolic changes in pre-infusion CAR T-cells predict response to therapy.*** (**a**) CLL patient (n = 14) CTL019 cells were stimulated overnight with beads coated with an isotype control (mock) or an anti-idiotypic antibody against CAR19. Extracellular lactate content was measured in culture supernatants. (**b**) Uptake of the fluorescent glucose analog 2-NBDG in mock- or CAR-stimulated retrospective patient CTL019 cells was assessed by flow cytometry (**a-b**, P values calculated using a paired two-tailed t-test). (**c**) Comparison of 2-NBDG uptake between responder (CR, n = 4; PR_{TD}, n = 2; PR, n = 2) and non-responder (NR, n = 6) CTL019 samples is shown. P values were determined with an un-paired two-tailed t-test. Bars depict mean ± s.e.m. (**d**) Representative flow cytometry showing the differentiation phenotype of CD8+ CAR T-cells following 9 days of culture in the absence (control) or presence of 2-DG which inhibits glycolysis. FMO = Fluorescence minus one. (**e**) Summary of subset (naïve-like: CCR7+CD45RO-; central memory: CCR7+CD45RO+; effector memory: CCR7-CD45RO+; effector: CCR7-CD45RO-) frequencies within CD8+ and CD4+ CAR T-cells following culture in the presence or absence of 2-DG is shown (n = 6; P values calculated with a two-tailed t-test). (**f**) Proliferative capacity of CTL019 cells manufactured in the presence or absence of 2-DG. CAR T-cells were serially re-stimulated with K562 cells engineered to express CD19 or mesothelin (irrelevant target antigen) on days 0, 7 and 12 of the culture, as indicated by the arrows. Data from 2 out of 5 representative subjects is shown (3 independent experiments).

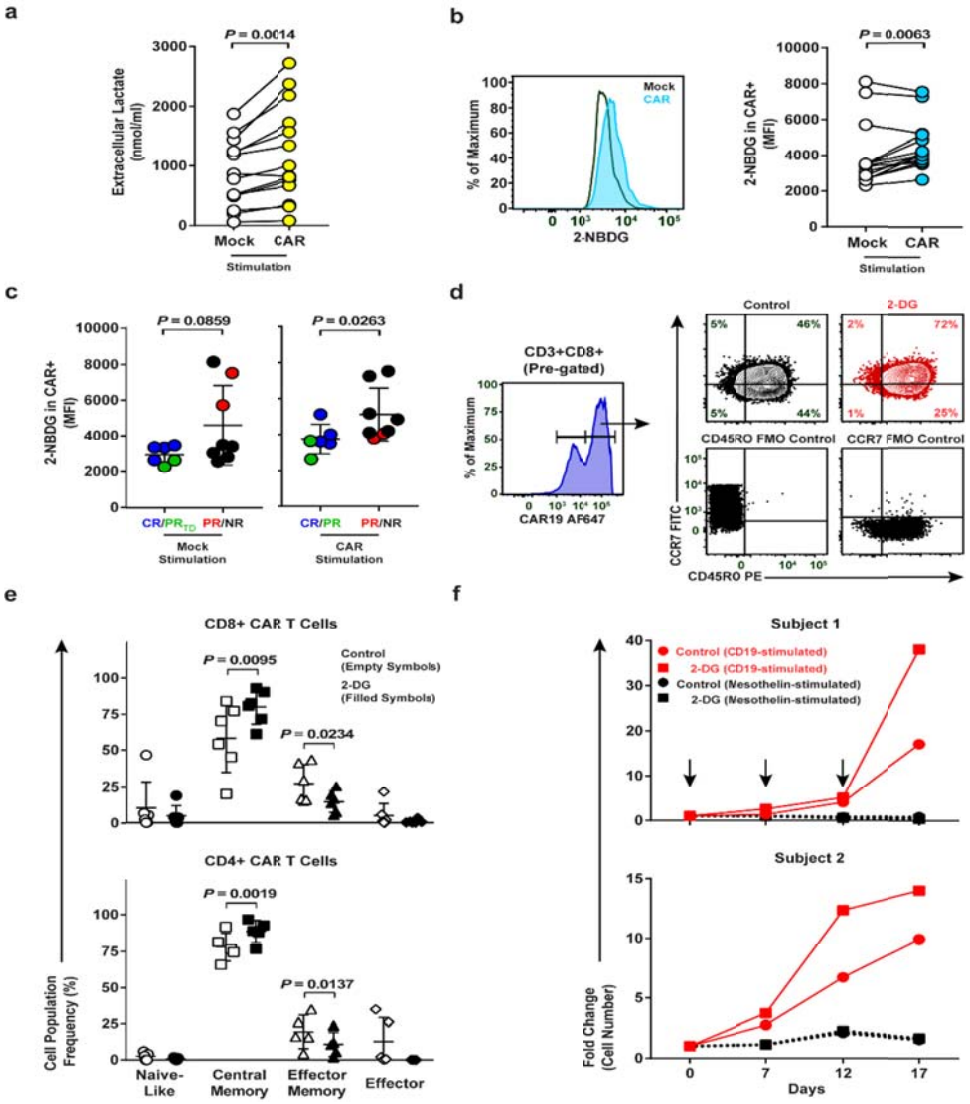

Supplemental Figure 3: ***Telomere length and telomerase activity of the CAR T-cell infusion product is not predictive of clinical response.*** (**a**) Comparison of telomere lengths between responder (CR, *n* = 8; PR_{TD}, *n* = 3; PR, *n* = 5) and non-responder (NR, *n* = 21) CTL019 samples, as determined by quantitative PCR. IMR-90 fibroblasts were cultured and harvested at different population doubling times to serve as controls for the detection of progressive telomere shortening. *P* values were calculated with a paired two-tailed *t*-test. (**b**) Spearman's rho correlation shown between relative T/S ratios measured by quantitative PCR and telomere lengths determined by Southern blot analysis of DNA samples prepared directly from pre-infusion CTL019 cells (*n* = 37). (**c**) Q-Trap assay for telomerase activity in CTL019 cells from 6 CLL patients. CAR T-cells were stimulated with beads coated with an isotype control antibody, αCD3/CD28 antibodies or an anti-idiotypic antibody against CAR19 (CR, *n* = 2; NR, *n* = 3; 3 replicates per patient sample). Mean ± s.d. shown. (**d**) Peak *in vivo* expansion of CTL019 cells in matched patients from panel **c** plotted as copies per microgram of genomic DNA.

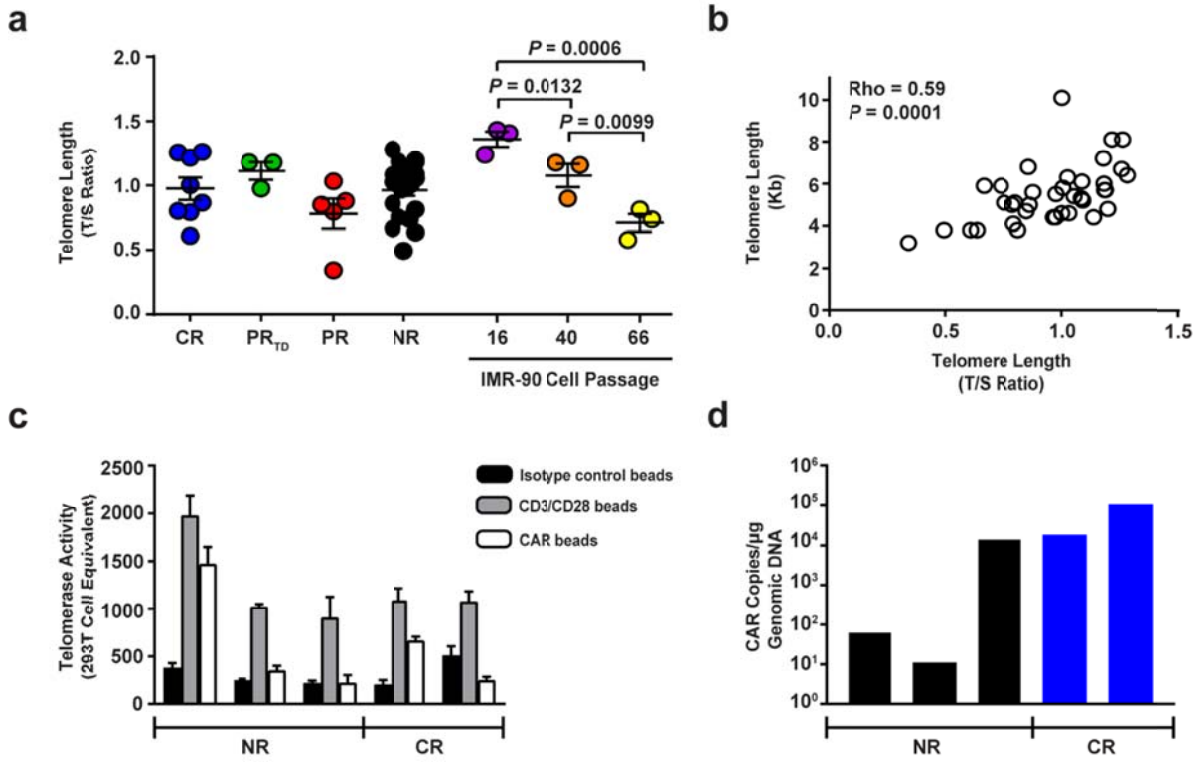

Supplemental Figure 4: ***Inhibition of the STAT3 pathway diminishes the proliferative capacity of CAR T-cells.*** (**a**) Representative flow cytometry showing levels of pSTAT3 in CTL019 cells that were stimulated overnight with isotype control beads (mock) or beads coated with an anti-idiotypic antibody against CAR19. CAR-specific stimulations were performed in the presence or absence of 5 µM Stattic, a small molecule inhibitor of STAT3 activation. (**b**) Expansion capacity of CTL019 cells generated in the presence or absence of 5 µM Stattic or an equivalent amount of DMSO (control). CAR T-cells from this representative subject (out of 8 different individuals) were then serially re-stimulated with K562 cells engineered to express CD19 on days 0, 7 and 12 of the culture, as indicated by the arrows. The fold change in CAR T-cell number from baseline is displayed (left *y*-axis) in parallel with cell viability (right *y*-axis). (**c**) Summary of cell proliferation and viability data on CTL019 cells from $n = 8$ different subjects (3 independent experiments) that were expanded with or without 5 µM Stattic prior to re-stimulation. The *P* value was calculated using a two-tailed Wilcoxon sign-rank test.

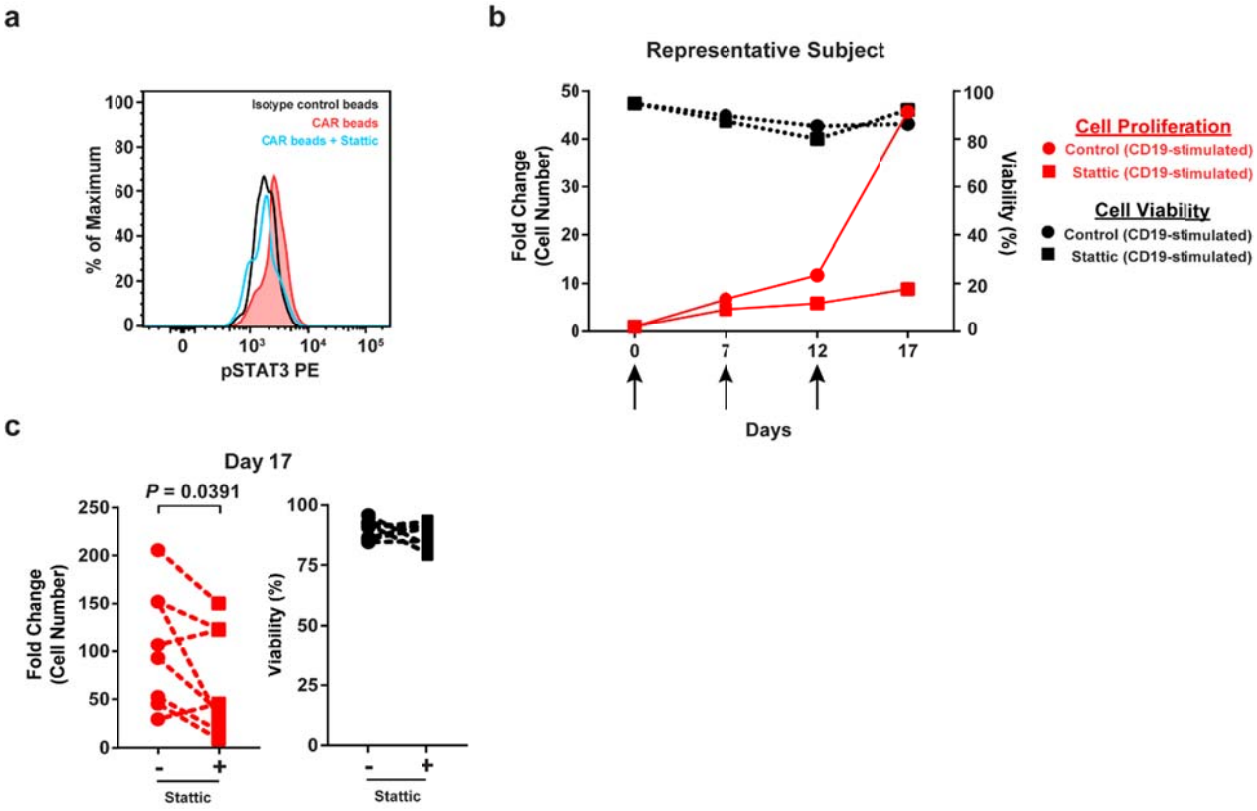

Supplemental Figure 5: ***Transcriptional profiles of leukapheresed T-cells in patients responding to CTL019 therapy are distinct from non-responders.*** (**a**) Genes differentially expressed in bulk, CD3+ T-cells from CLL patients who responded to CTL019 therapy (CR + PR_{TD}; *n* = 3) or non-responding subjects (NR; *n* = 11). Retrospective apheresis samples from patients belonging to the PR group were not available. Each column represents a sample from an individual patient and each row an individual gene, colored to indicate normalized expression. The top 200 genes in either direction are shown. (**b**) Heat map of selected pathways significantly enriched in genes induced or repressed in *ex vivo* CD3+ T-cells from patients belonging to each response group is displayed. A color gradient ranging from dark red to dark blue depicts the gene set enrichment score of pathways enriched in genes induced (red) or repressed (blue). *P* values were calculated using a two-tailed Welch's *t*-test comparing CR + PR_{TD} patients (as one group; *n* = 3) to NR subjects (as one group; *n* = 11).

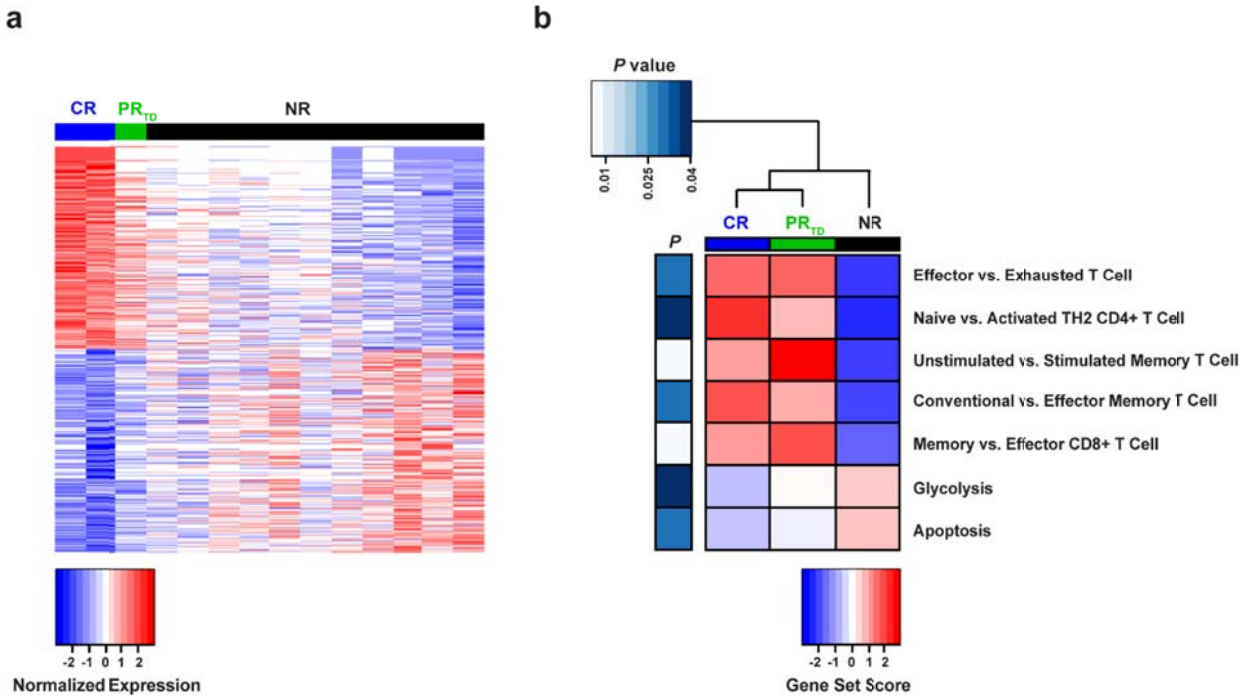

Supplemental Figure 6: ***CITRUS analysis of leukapheresed CD8+ T-cells reveals cell populations characterized by elevated levels of CD27 and low levels of CD45RO expression that segregate CR/PR$_{TD}$ from PR/NR patients.*** Unsupervised hierarchical clustering of populations (**a** and **b**, top) based on the median expression levels of phenotypic markers measured across the cells for each population is shown. Red clusters were identified as being the strongest differentiating populations between (**a**) CR/PR$_{TD}$ and PR/NR or (**b**) CR and NR patient groups based on a supervised learning algorithm that determines the clusters and features which best predict endpoint stratification. Phenotype plots of CD8+ T cell populations (clusters) that are the best segregators of (**a**), CR/PR$_{TD}$ from PR/NR and (**b**) CR from NR response groups are shown. CD27 and CD45RO were identified in all population clusters as having prognostic utility. For panels **a** and **b**, (CR, n = 7; PR$_{TD}$, n = 3; PR, n = 4; NR, n = 24). Boxes represent 25-75 percentiles; the middle line indicates the median and whiskers denote min. to max. Each symbol represents an individual patient sample.

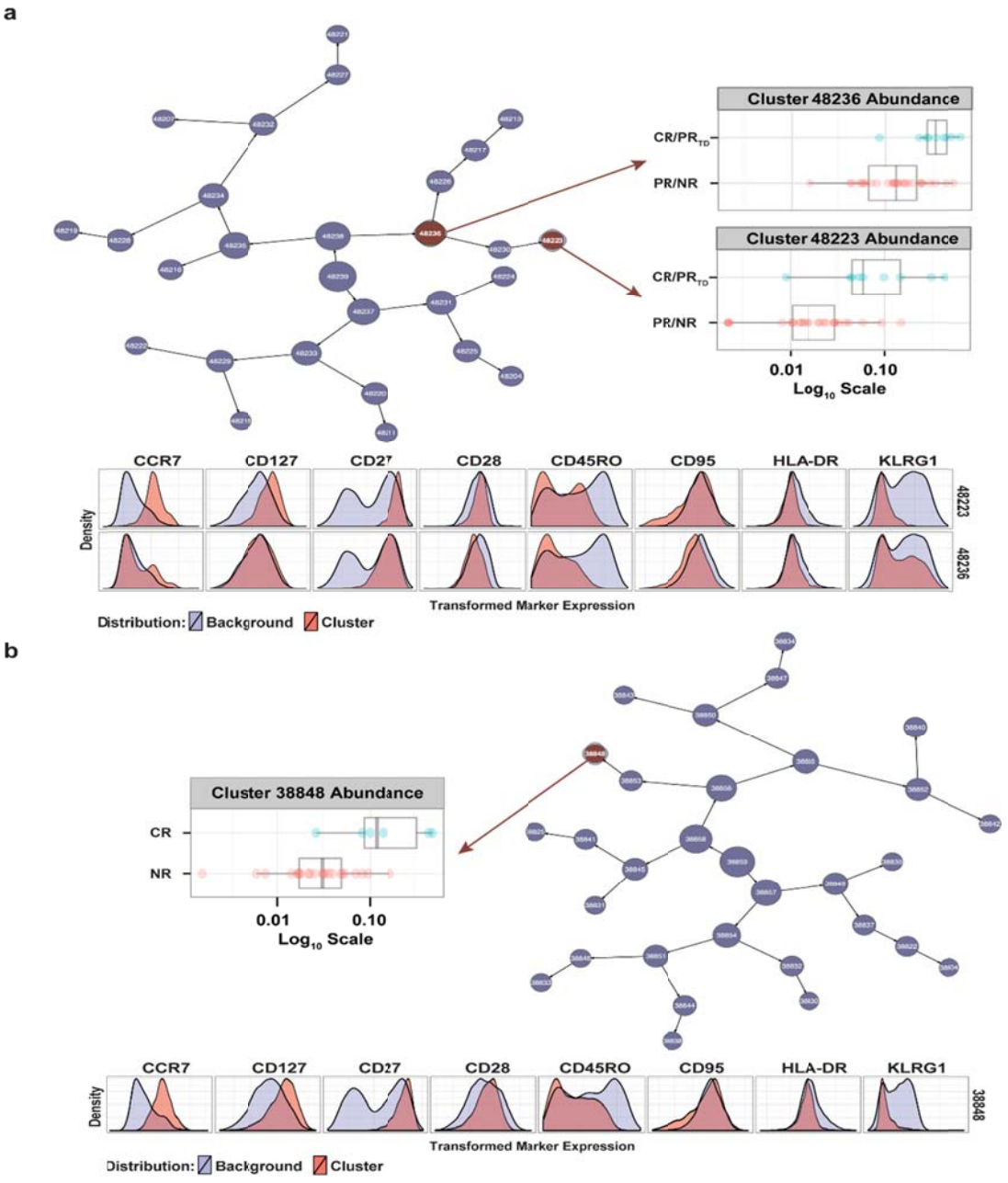

Supplemental Figure 7: ***CLL patient CD45RO-CD27+ CD8+ T-cells possess attributes of conventional memory T-cells.*** (**a**) Histograms showing CCR7 expression on CD8+ T cell subsets of a representative CLL patient at the time of leukapheresis (left) and summarized data for $n = 38$ subjects (right). *P* values were calculated using a Wilcoxon sign-rank test. Mean ± s.e.m. is depicted. (**b**) CFSE dilution in CD8+ T cell subsets after stimulation with αCD3/CD28 beads for 5 days (representative data of 3 different subjects; 2 independent experiments). Data are shown after gating on live CD8+ T-cells. (**c**) Differentiation phenotype (naïve-like: CCR7+CD45RO-; central memory: CCR7+CD45RO+; effector memory: CCR7-CD45RO+; effector: CCR7-CD45RO-) of sorted CD8+ T cell subsets following CD3/CD28 stimulation for 5, 9 and 13 days ($n = 3$ subjects). Pie chart slices indicate frequencies of each population according to the differentiation phenotype. (**d**) IL-2 production from CD8+ T cell subsets from $n = 3$ different subjects stimulated with beads coated with an isotype control (mock) or αCD3/CD28 antibodies for 24 hours. Error bars represent s.e.m. (**e**) Cytolytic capacity of CTL019 cells generated from sorted T-cell subsets following 18 hours of co-culture with NALM-6 tumor targets at the indicated effector:target cell ratios. Mean ± s.e.m. shown (pooled data from $n = 3$ subjects). (**f**) Representative patient histogram (left) and mean fluorescence intensity (MFI) of intracellular granzyme B in CD27+CD45RO- CD8+ T-cells relative to CD27+CD45RO+ CD8+ T-cells. (**g**) Representative flow cytometry (left panel) and frequency of *ex vivo* CD27+CD45RO- CD8+ T-cells expressing Ki-67 compared to their CD27+CD45RO+ counterpart (right). Graphs show mean and s.e.m. (**f-g**; $n = 38$) *P* values were determined using a two-tailed paired *t*-test.

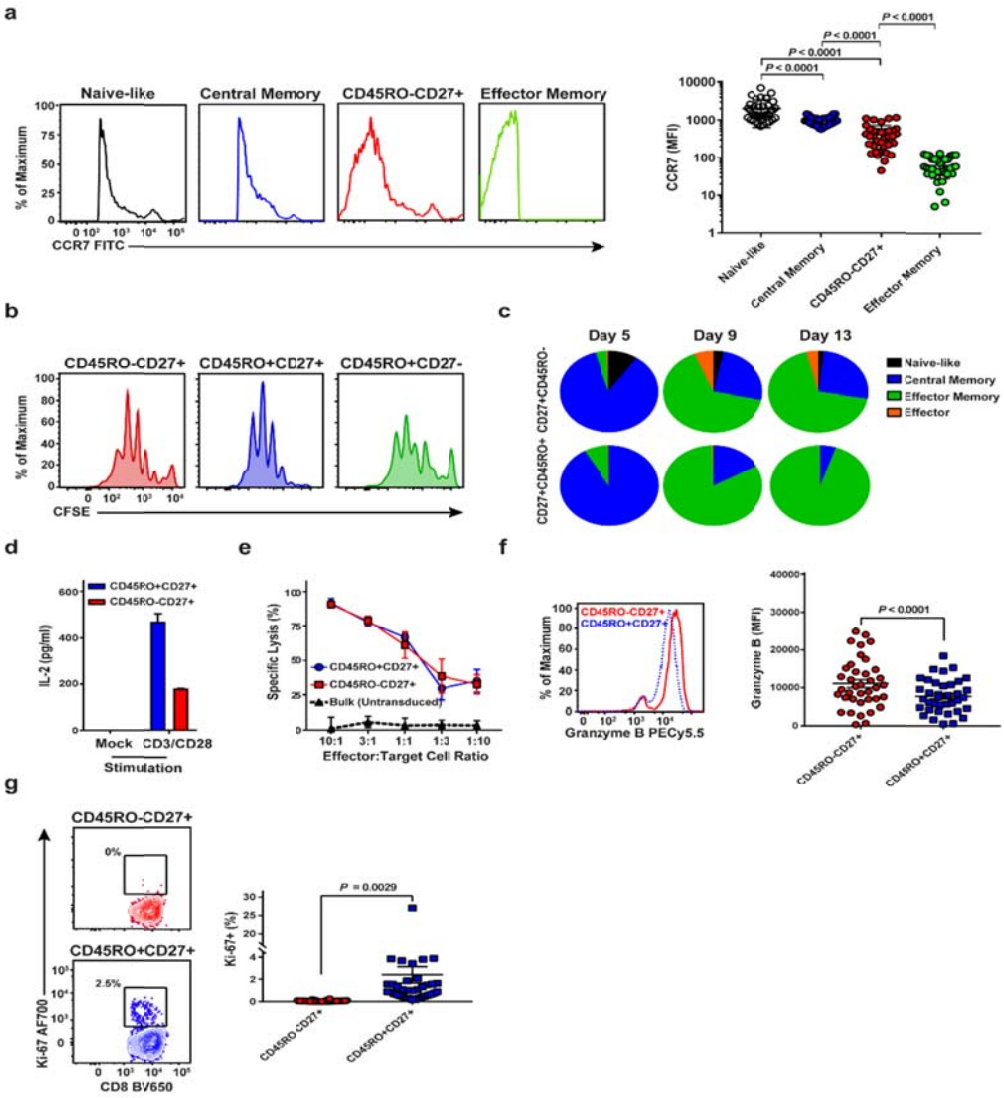

Supplemental Figure 8: ***CD4:CD8 ratio in pre-infusion CLL patient CAR T-cells is not predictive of response.*** Comparison of CD4:CD8 ratio in leukapheresis samples and CTL019 products across response groups (CR, $n = 7$; PR_{TD}, $n = 3$; PR, $n = 4$; NR, $n = 25$). Graph shows mean and s.e.m. A Wilcoxon sign-rank test was used for evaluating significant differences in the CD4:CD8 ratio between leukapheresis samples and patient-matched cellular infusion products.

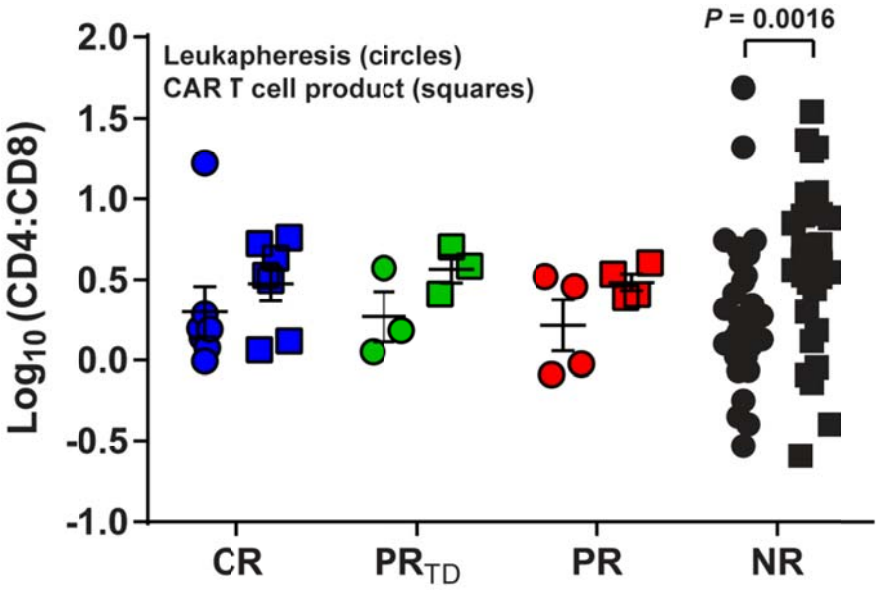

Supplemental Figure 9: ***The frequency of CD8+ T-cells expressing inhibitory receptors at the time of leukapheresis does not predict clinical outcome.*** Percentages of leukapheresed CLL patient CD8+ T-cells expressing (**a**) PD-1 and co-expressing (**b**) LAG-3 or (**c**) TIM-3 compared across response groups (CR, $n = 6$; PR_{TD}, $n = 3$; PR, $n = 4$; NR, $n = 25$). Graphs depict mean ± s.e.m.

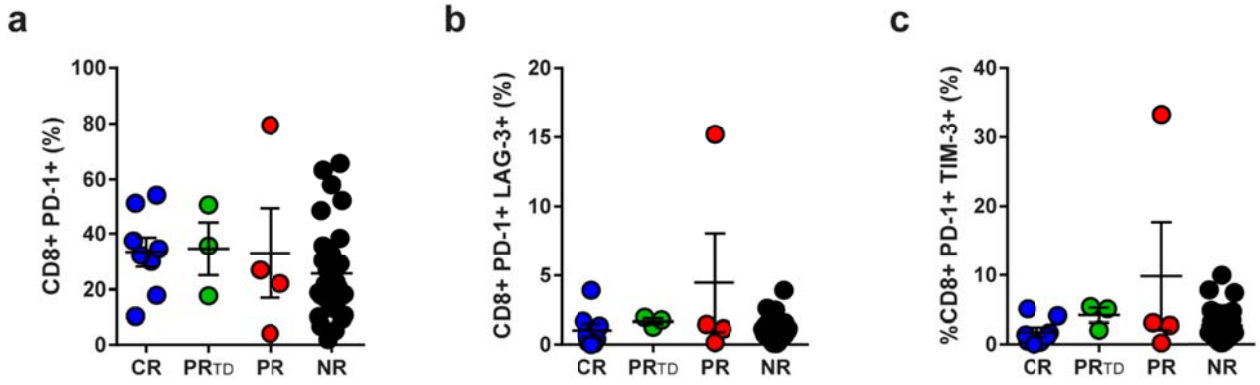

Supplemental Figure 10: Receiver operating characteristic (ROC) curves demonstrate that patients infused with high doses of CD8+CD27+PD-1- CAR T-cells respond to therapy. ROC curves are based on total doses of CAR T-cells (cells/kg) possessing different phenotypes that were infused into responding (n = 14) versus non-responding (n = 21) patients. Areas under the curve (AUCs) provide a measure of predictive power for each biomarker population.

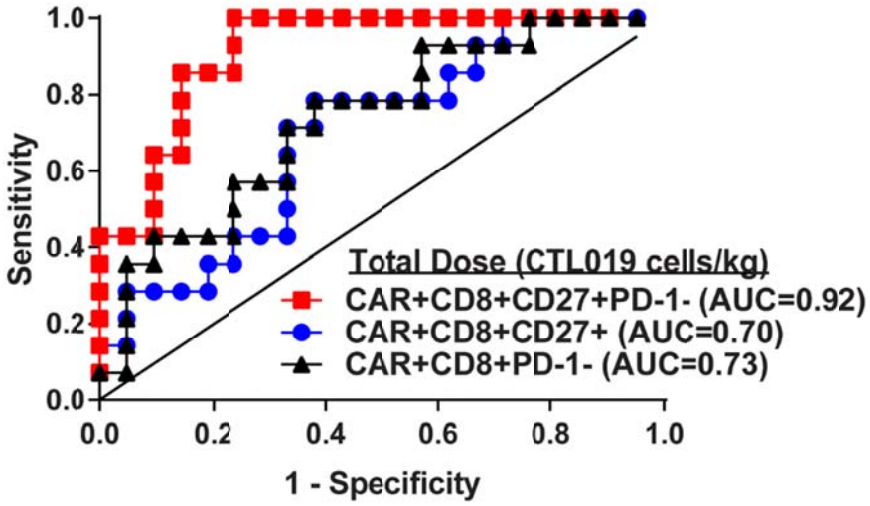

Supplemental Figure 11: CD27+PD-1- CD8+ T-cells exhibit high levels of pSTAT3 in response to IL-6 as compared to other sub-populations. (**a**) Representative histograms (left) showing levels of pSTAT3 in CD8+ T cell populations that were purified by fluorescence-activated cell sorting and stimulated with recombinant IL-6 (10 ng/ml). Summary of IL-6-induced pSTAT3 levels in CD8+ T cell subsets defined by CD27 and PD-1 expression from $n = 4$ different subjects (right). The change in mean fluorescence intensity (ΔMFI) was determined by subtracting the MFI of pSTAT3 in IL-6-treated cells

from the same parameter in matched, unstimulated cells. (**b**) Example flow cytometry (left) and pooled data from n = 7 different subjects (right) showing levels of the interleukin-6 receptor subunit beta (CD130) in CD8+ T cell populations defined by CD27 and PD-1 expression. P values were calculated using a two-tailed paired t-test.